Timing is (almost) everything in a comprehensive, spike-resolved flight motor program

Rachel Conn[1,2†], Joy Putney[3†], Simon Sponberg[1,3*]

[1]School of Physics, Georgia Institute of Technology, Atlanta, GA, 30332 USA
[2]Neuroscience Program, Emory University, Atlanta, GA, USA
[3]School of Biological Sciences & Graduate Program in Quantitative Biosciences,
Georgia Institute of Technology, Atlanta, GA, 30332 USA

[†]**These authors contributed equally to this work.**

[*]**Correspondence:**
Dr. Simon Sponberg
Georgia Institute of Technology
School of Physics & School of Biological Sciences
Atlanta, GA 30332, USA
sponberg@gatech.edu

Abstract

Precise spike timing can be critical in sensory systems. In a few specific motor systems, we now know millisecond-scale timing of neural spikes is functionally important for behavior. However, we know little about the extent of timing codes across the whole motor program of an animal. Taking advantage of the relatively few motor units that control the wings of a hawk moth, we captured a comprehensive, spike-resolved motor program in tethered flight. We simultaneously record nearly every action potential from all muscles and the resulting forces. We find that timing encodes more information than rate in every motor unit. Motor units use consistent encoding, blending precise spike timing and rate information in a 3:1 ratio, despite their varying functions. Finally, we show that each muscle is coordinated with all other muscles through spike timings while spike rates are independent. Spike timing codes are ubiquitous, consistent, and essential for coordination.

Introduction

Neurons convey information through both rate and temporal codes [1–3]. Both the firing rate and the precise, millisecond-level sequences of spikes are well established as essential encoding mechanisms for sensory systems in the periphery and cortex for proprioception [4], audition [5], vision [6], touch [7], and other modalities [8, 9]. Rate codes are thought to be the predominant strategy used by motor systems in part due to the presumed slow, low-pass nature of muscle force production and recruitment principles [10–12]. However, recent evidence show that precise spike timings may be under-appreciated for controlling motor behaviors at least in specific muscles or motor circuits [3]. Temporal codes have been found in a songbird cortical area for vocalization [13] and in mouse cerebellum for task error correction [14]. Correlational, causal, and mechanistic studies in biomechanics and muscle physiology show that millisecond-level changes in timing of spikes in motor neurons can manifest profound changes in force production and even behavior selection [15, 16]. Temporal encoding is not only present in fast behaviors like invertebrate flight, but also in relatively slow behaviors like breathing in birds [17]. However, evidence for the importance of timing codes has been limited to only a few of the motor signals that typically control movement. Whether temporal codes are utilized broadly across a complete motor program for behavior is unknown as is their role in coordinating multiple motor units. Despite growing appreciation of the potential for motor timing codes, we have not yet established the ubiquity, consistency and coordination of timing strategies compared to rate codes across the motor signals that compose a behavior.

Timing codes may be restricted to only a few motor signals that control behavior. For example, recordings of small sets of muscles in locusts, hawk moths, and fruit flies have shown that spike timing and rate variation are prevalent in specific motor units, and that not all muscles have significant timing variation [18–20]. Alternatively, timing codes may be ubiquitous–widespread across the entire motor program and present in all muscles controlling a behavior. Regardless of the prevalence of timing codes, individual motor neurons within the population may exhibit specialized encoding strategies, varying the amount of timing and rate information depending on the function of the muscles they innervate. For example, *Drosophila* appear to use combinations of functionally distinct phasic and tonic motor units to control flight [21]. Additionally, evidence in sensory systems show separate classes of neurons use either rate or temporal encoding to convey sensory information [22]. Alternatively, timing and rate encoding strategies may be consistently employed across the entire motor program. Finally, coordination of multiple motor signals is typically assessed through covariation in muscle rates. For example, motor coordination patterns across muscles (*e.g.* muscle synergies [23]) and population recordings of M1 neurons in motor cortex (*e.g.* [24]) all consider movement encoding in populations of rate codes. Alternatively, coordination of muscles may be achieved by sharing information in the motor system through timing codes. Resolving these hypotheses is challenging because they consider the patterns of encoding across the entire motor program. It is therefore necessary to record from a spike-resolved, comprehensive set of motor signals that control a behavior simultaneously in a consistent behavioral context.

Recording a comprehensive motor program is technically challenging due to the requirements of completeness, sufficient temporal resolution, and sampling rich variation. Obtaining a nearly complete motor program is more tractable in the peripheral nervous system than in cortex because of smaller neuronal population sizes. While many muscles or motor units have been simultaneously recorded using electromyography (EMG) in frogs [25], cats [23], and humans [26] and using calcium imaging in the wing steering muscles of fruit flies [21], these sets of neural signals are not spike-resolved, so they lack sufficient temporal resolution to fully investigate the relative importance of rate and temporal codes. Large flying insects are especially feasible organisms in which to record a spike-resolved, comprehensive motor program because all muscles actuating the wings are in the thorax, there are relatively few muscles compared to many segmented limbs, and flight muscles frequently function as single motor units: they are generally innervated by one or very few fast-type motor neurons with a 1:1 relationship between muscle and neural potentials [27, 28].

We take advantage of this opportunity by capturing a spike-resolved, comprehensive motor program in a hawk moth, *Manduca sexta*, and leveraging it to investigate the importance of temporal encoding in a nearly complete population code for movement. Many muscles in the hawk moth motor program are known to exhibit variation in both timing and rate of muscle activation during turning maneuvers in flight [20, 29–31]. This rich, nearly complete motor program enables us to address three questions about timing codes in motor systems: First, do all muscles encode flight behavior using precise spike timings? Second, do muscles use different or consistent strategies to encode flight behavior? Finally, how do rate and timing codes allow for coordination across muscles?

Results

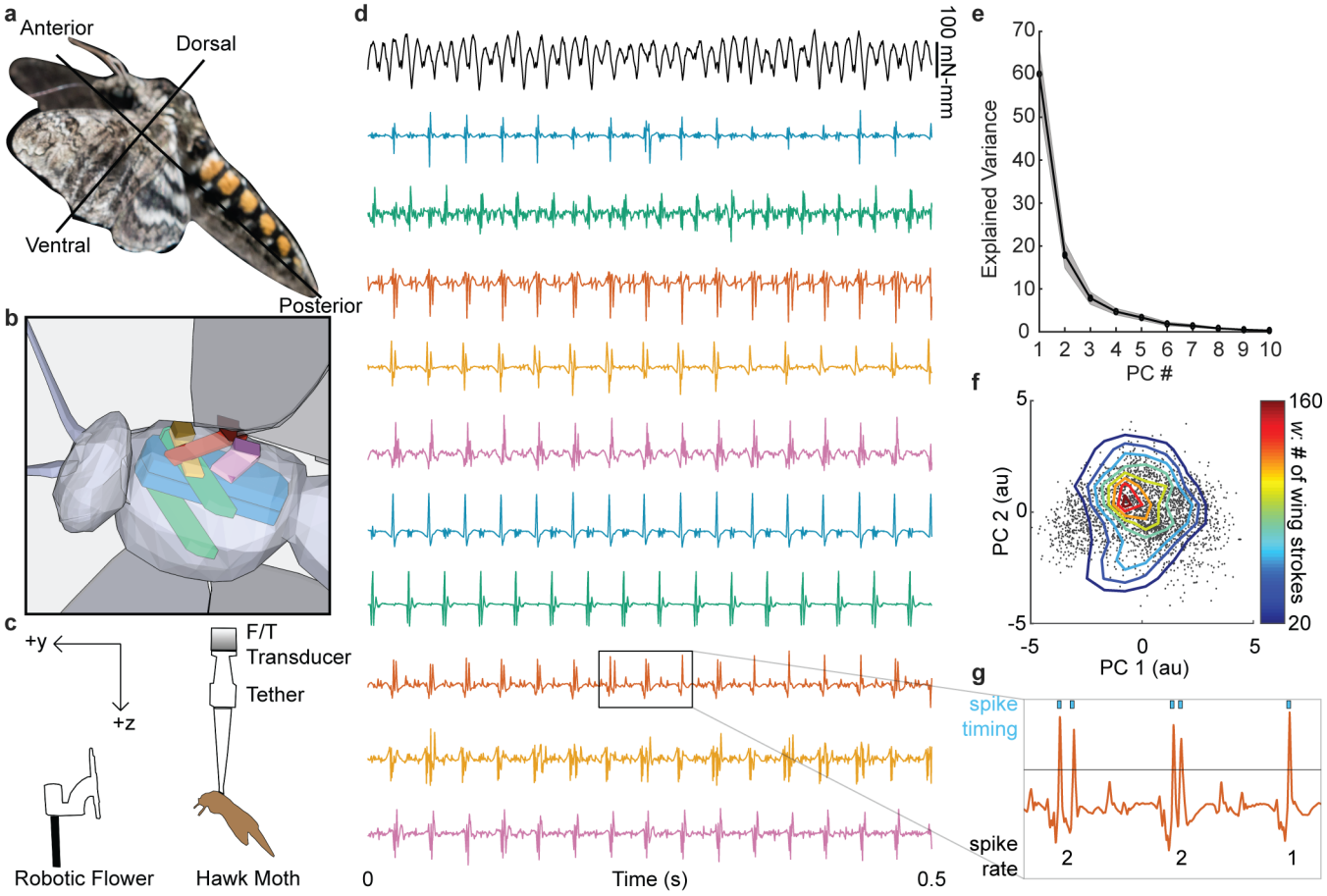

Figure 1 | **EMGs from 10 flight muscles and simultaneous yaw torque.. a,** A hawk moth, *Manduca sexta*, in flight. **b,** A simplified 3D sketch of the 5 bilateral pairs of muscles from a ventrolateral view: dorsolongitudinal, DLM (blue); dorsoventral, DVM (green); 3rd axillary, 3AX (orange); basalar, BA (yellow); subalar, SA (purple). Muscles on the left and right sides of the animal are distinguished with an L or an R (ex. L3AX). **c,** Hawk moths experienced visual stimuli from a robotic flower oscillating with a 1 Hz sinusoidal trajectory while tethered to a custom six-axis F/T transducer (N = 7 moths; 999-2,954 wing strokes per moth; average per moth = 1,950 wing strokes). **d,** EMG (color scheme as above) and

yaw torque (black) from 0.5 seconds of flight. **e,** The first two principal components (PCs) of the yaw torque waveforms captured most of the variance (mean, in black; $\pm$ S.E.M., in gray; N = 7 moths). **f,** Projection of yaw torque onto the first two PCs for each wing stroke from a moth (w = 2,739 wing strokes) in PC space (arbitrary units, au). The joint histogram of the distribution is represented in a 10 x 10 grid between -5 and 5 using isoclines from the contour function in MATLAB (MathWorks). **g,** Spike sorting was accomplished using threshold crossing (e.g. black line) in Offline Sorter (Plexon). Spike rate is the number of spikes in each wing stroke, and spike timing is the precise spike time relative to the start of each wing stroke.

Spike rate information is present, but timing information is ubiquitous in the motor program

We recorded a comprehensive motor program with spike-level resolution across all the primary muscles actuating the wings in a hawk moth (*Manduca sexta*, N = 7) (Fig. 1a). The hawk moth musculature has been examined in detail anatomically and through *in vivo* and *in vitro* recordings (see Supplementary Text). Based on this rich literature we identified and recorded EMG signals from five bilateral pairs of muscles that have important roles in controlling the wings during flight (Fig. 1b; S1, S2). We simultaneously obtained within-wing stroke yaw torque using a custom force-torque transducer (ATI) in tethered flight while the moth visually tracked a robotic flower (Fig. 1c,d) [15, 32]. We segmented our data into wing strokes, and used principal components analysis (PCA) to reduce the dimensionality of the yaw torque waveforms. The first two PCs explained most of the variance ($78.0 \pm 4.0\%$) in yaw torque across wing strokes (Fig. 1e). The visual stimulus elicited variation in the moths' motor output, sampling a broad range of yaw turns (Fig. 1f). We treated each wing stroke as an independent sample of the spiking activity as spike rate or spike timing in the 10 muscles and the yaw torque (Fig. 1g).

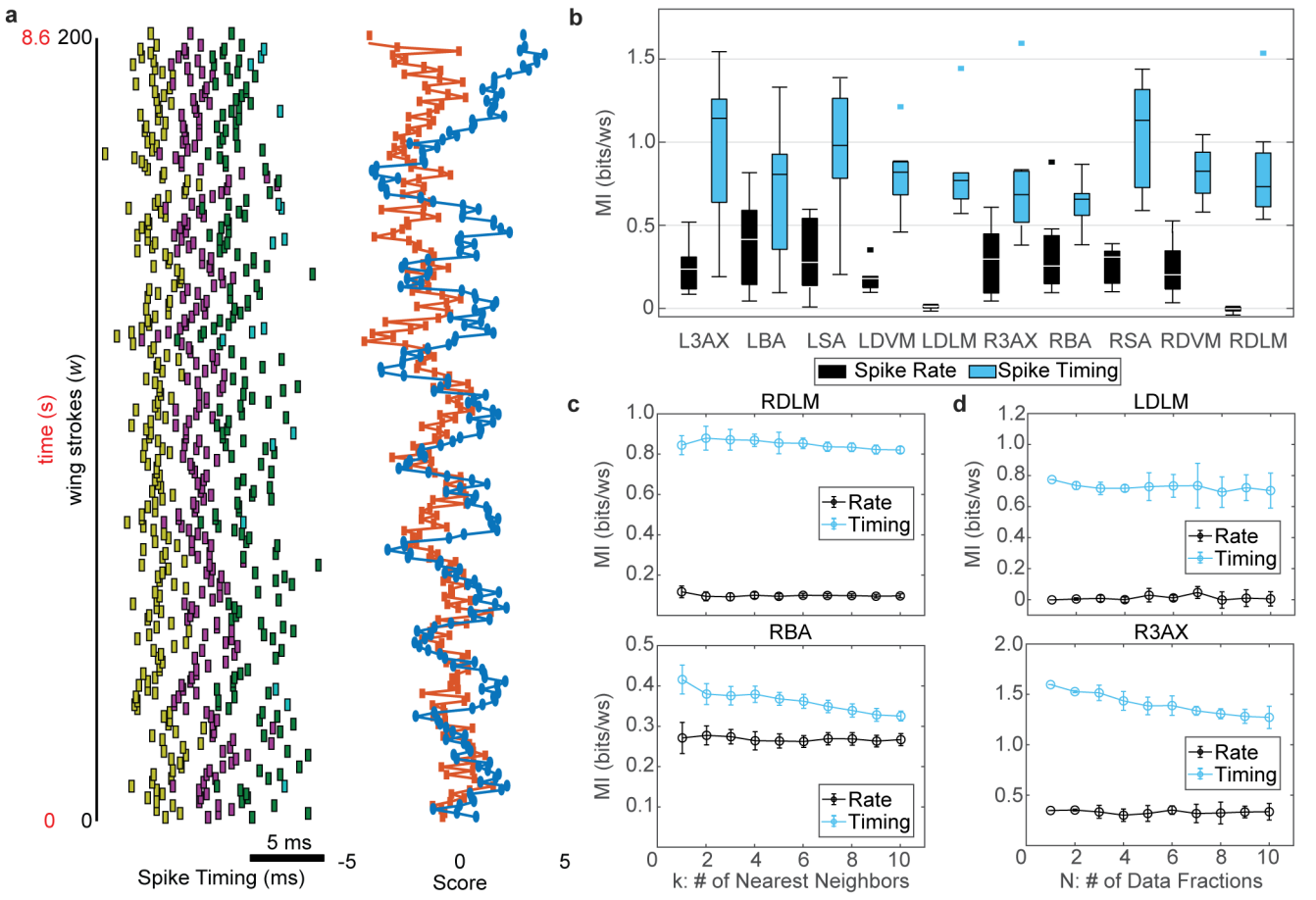

Figure 2 | **Mutual information between spike rate or spike timing and yaw torque. a,** Timing of spikes in the L3AX and PC scores show variability corresponding with the 1 Hz visual stimulus (200 wing strokes). The rasters are the 1st (yellow), 2nd (purple), 3rd (green), and 4th (light blue) spikes within each wing stroke shown alongside the 1st (blue) and 2nd (red) yaw torque PC scores. **b,** MI estimates for spike rate (black) and spike timing (blue) with yaw torque across individuals (N = 7). Box plots report the median as the center line in the box, which marks the 25th and 75th percentiles. Whiskers are range of all points that are not considered outliers (square points). Spike rate MI is less than spike timing MI (two-way ANOVA comparing timing vs. rate for all muscles: rate vs. timing, p

$< 10^{10}$; muscle ID, p = 0.26; interaction, p = 0.09). Spike timing MI is significantly greater than spike rate MI in most paired comparisons within muscles (paired t-tests: $p < 0.02$ for all muscles except the LBA, p = 0.09, and RBA, p = 0.05. Wilcoxon signed rank tests: $p < 0.02$ for all muscles except the LBA, p = 0.11, and RBA, p = 0.08). **c,** MI estimates (mean $\pm$ S.D.) for the number of nearest neighbors k = 1-10 from the RDLM and RBA muscles of one moth [33, 34]. **d,** MI estimates (mean $\pm$ S.D.) for data fractions N = 1-10 from the LDLM and R3AX muscles of one moth.

Both the spike rate and the timing of individual spikes within the muscles show modulation along with the motor output (Fig. 2a). To test the separate contributions of rate and temporal encoding in individual muscles, we estimated the mutual information between muscle activity and yaw torque. We separated spike rate mutual information (MI) and spike timing MI by conditioning spike timing on spike rate [17]:

$$I(S;\tau) = I(S_r;\tau) + \sum_{i=1}^{S_{r,max}} p(S_r = i) I(S_t;\tau|S_r = i) \quad (1)$$

Here, I corresponds to MI. S_r corresponds to spike rate, or the total number of spikes in each wing-stroke. τ is the moth's yaw torque represented as the first two PCs. i represents each spike rate condition, and $p(S_r = i)$ is the probability of the spike rate condition. The two terms of this equation correspond to the spike rate MI and spike timing MI, respectively (see Online Methods). We used the Kraskov k-nearest neighbors method to estimate both MI values [33, 34].

For all 10 muscles, spike timing MI is higher than spike rate MI for informing yaw torque motor output (Fig. 2b). In all muscles both spike rate MI and spike timing MI are non-zero, except for the DLM, which only spikes once per wing stroke during flight (range of mean spike rate MI across 10 muscles = 0.0 - 0.4 bits/wing stroke (ws); spike timing MI = 0.6 - 1 bits/ws). All muscles in the motor program that vary the number of spikes present in each wing stroke use mixed encoding strategies, combinations of spike timing and spike rate to inform the torque. The error estimates (see Online Methods) of the MIs were small compared to the total MI (Table S1, spike rate and timing MI error < 0.04 bits/ws across all muscles). Our MI estimates are stable across varying values of *k*, the number of nearest neighbors, and the number of data fractions (Fig. 2c,d; S3, S4). In the spike timing MI estimations, 90% of estimations from halved data sets deviated by less than 10% from the full data set estimate.

Temporal encoding is ubiquitous across the entire flight motor program, present in every muscle, and is utilized more than rate encoding (Fig. 2b). Each motor unit encodes almost an order of magnitude more information about yaw torque in precise spike timings (0.8 bits/ws on average for all muscles) compared to other systems, like a cortical vocal area (between 0.1-0.3 bits/syllable) [13] and breathing muscles (between 0.05-0.2 bits/breath cycle) of song birds [17]. However, the moth's individual motor units still encode on the order of 1 bit per wing stroke, though they collectively code for the wide variety of torque behaviors the moths perform.

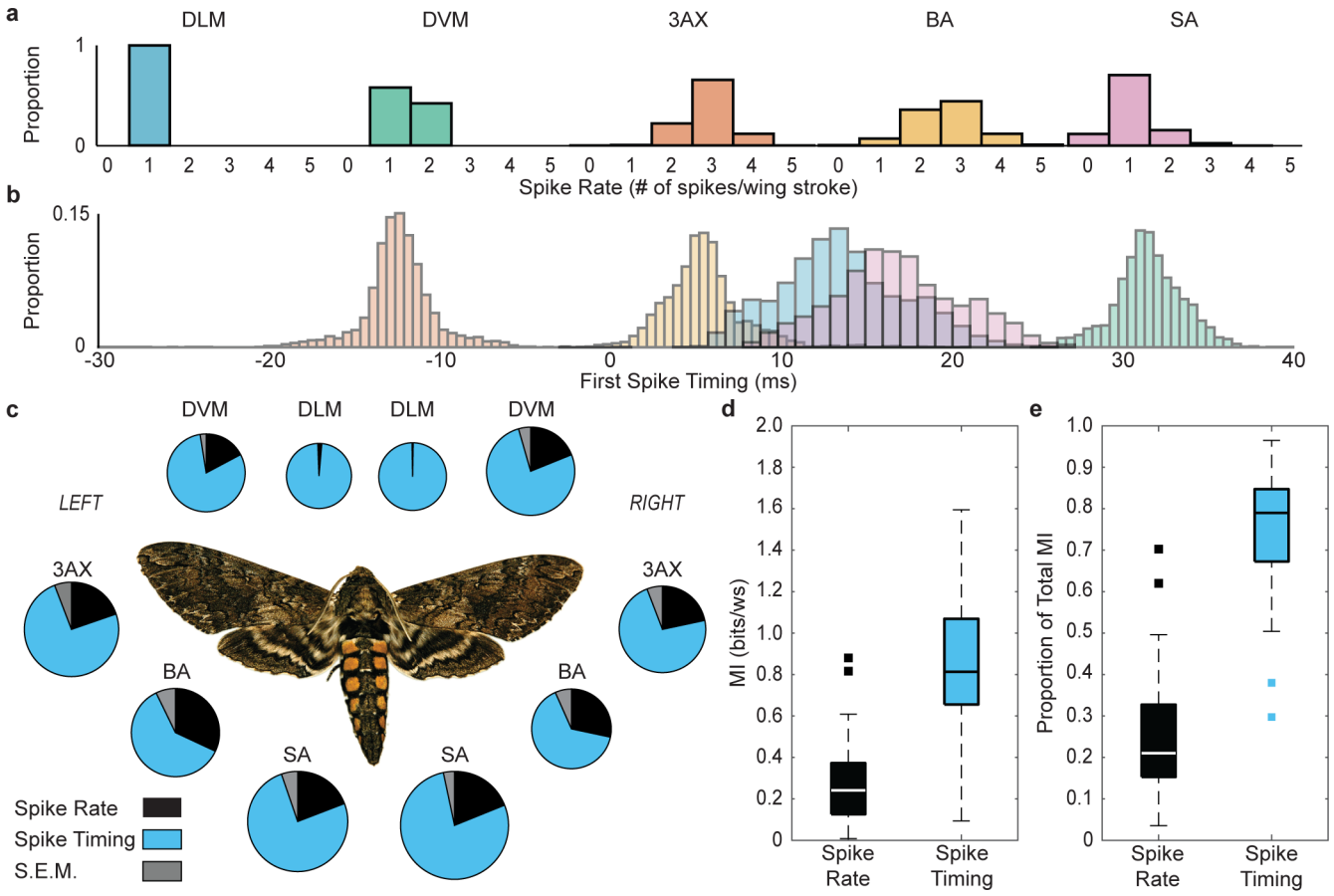

Figure 3 | Consistency of magnitude and proportion of spike timing MI and spike rate MI across all 10 muscles. a, The 5 muscle types we recorded have different probability distributions of spike rate conditions (data shown for one moth). **b,** There is variation in the probability distributions of the first spike timing across the 5 muscle types (data shown for one moth). Some bursts begin before the wing stroke and continue into the wing stroke; these were reported as negative values (t = 0 corresponds to the start of the wing stroke). **c,** Mean spike rate and spike timing MI estimates for all 10 muscles across individuals (N = 7). Pie size indicates the magnitude of total MI, and the slices indicate the proportion that is spike rate (black) and spike timing (blue), as well as the S.E.M. these proportions (gray). No

significant difference was found in the magnitude of spike rate MI of all muscles excluding the DLM (one-way ANOVA: $p = 0.66$; Kruskal-Wallis test: $p = 0.90$) or spike timing MI of all muscles (one-way ANOVA: $p = 0.54$; Kruskal-Wallis test: $p = 0.39$). No significant difference was found in the proportion of spike timing MI to total MI in all muscles excluding the DLM (one-way ANOVA: $p = 0.31$; Kruskal-Wallis test: $p = 0.54$). **d,e,** The magnitude or proportion of spike rate MI (black) and spike timing MI (blue), respectively, across 8 muscles (DLM excluded) and 7 individuals. Boxplots display data as previously described in Fig. 2b.

Encoding strategy is consistent across functionally diverse muscles

Muscles in the hawk moth motor program exhibit extensive diversity in their biomechanical functions. For example, the main indirect downstroke muscle (dorsolongitudinal muscle, DLM), acts by pulling on the exoskeleton at each end to contract the thorax. Mechanical strain from the contracting exoskeleton propagates to the wing hinge and causes the wings to depress [20]. In contrast to the DLM, the third axillary muscle (3AX) directly affects the wing position by pulling on the third axillary sclerite, which articulates the anal vein, the most posterior vein of the forewing [31, 35]. In addition to functional differences, muscles exhibit distinct patterns of variation in their spiking activity. Different muscles have different ranges of spike count per wing stroke (i.e. spike rate) and different amounts of timing variation during the wing strokes (Fig. 3a,b).

Despite their diverse properties, the 10 muscles in the motor program of the hawk moth are consistent in the magnitude and proportion of rate and timing information used to encode yaw torque (Fig. 3c). No muscle carries significantly different spike timing MI. Additionally, all muscles that spike more than once per wing stroke carry similar amounts of spike rate MI.

As a result, there is no significant difference between the 3:1 ratio of spike timing MI to spike rate MI for all muscles that spike more than once per wing stroke (Fig. 3c-e: mean $\pm$ S.E.M. of the ratio of spike timing MI to total MI for all muscles excluding DLM = 0.75 ± 0.01). There is evidence that neurons in the sensory system may use distinct strategies to encode particular types of information [22]. However, this is not the case in the peripheral motor program for *Manduca sexta*. Despite the differences in

188 biomechanics and firing pattern statistics, muscles in the moth motor program exhibit consistent use of
189 temporal and rate encoding strategies. The moth's nervous system uses a consistent code for turning
190 behavior. It may seem surprising that though each muscle has a different probability distribution of
191 spike rate and spike timing, each muscle has a comparable amount of MI with the moth's torque. The
192 different probability distributions may indicate that different muscles have varying amounts of total
193 entropy (bandwidth) while still transmitting the same information. An alternative explanation may be
194 that different muscle types have comparable total entropies, but they encode torque with varying
195 temporal and rate precision.

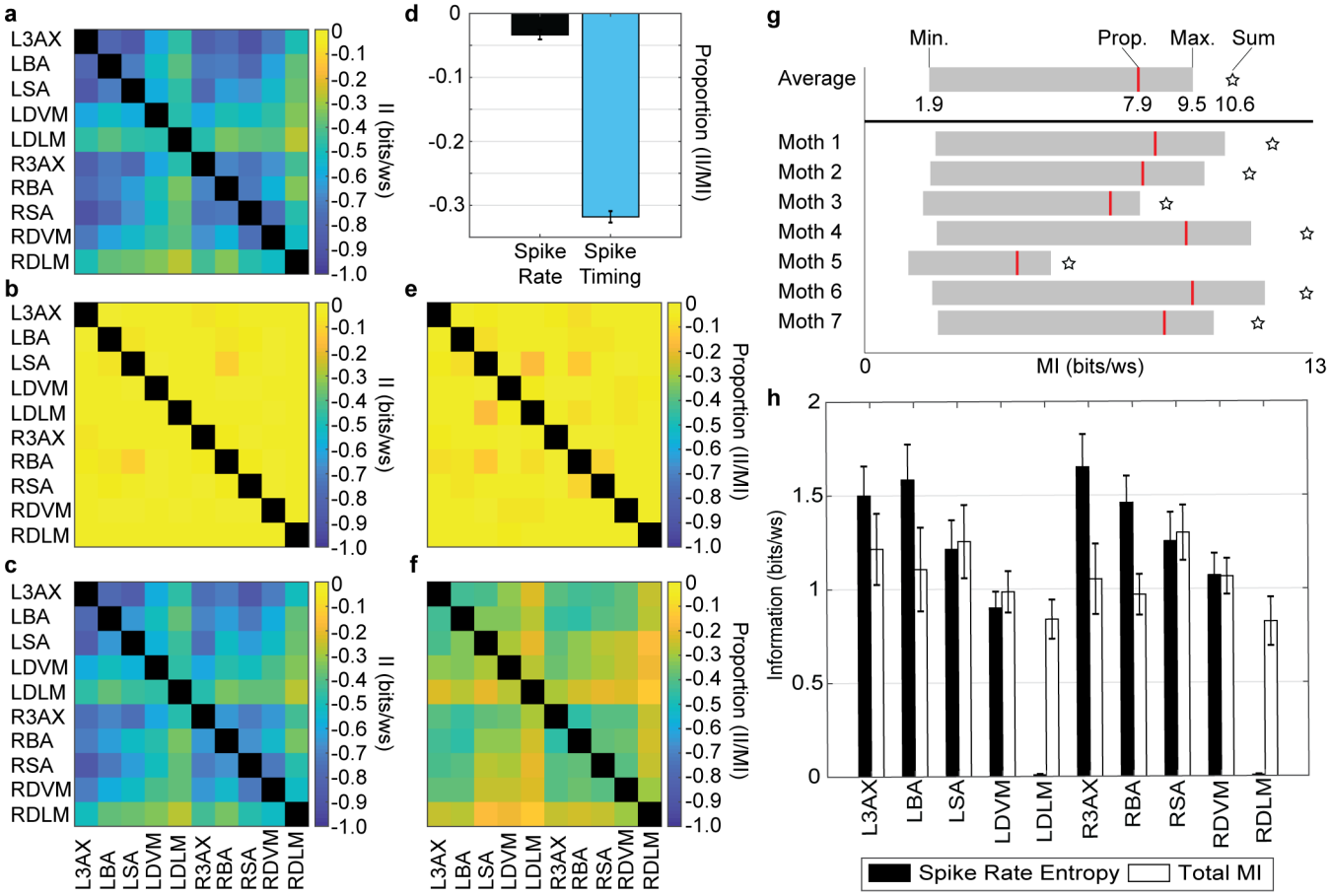

Figure 4 | Interaction information in pairwise combinations of muscles and the range of total motor program MI values possible. a, We calculated total interaction information (II) (Equation (3)) [36] as a measure that compares the estimates of pairwise MI (Equation (2)) and individual muscle MI (Equation (1)) for all pairwise combinations of muscles (mean for N = 7 moths). All values of II are negative, indicating net redundant interactions or overlapping information content. Comparisons of muscles to themselves are excluded. **b,c** Spike rate interaction information (II_{rate}) or spike timing interaction information (II_{timing}), respectively, across all pairwise combinations of muscles (Equation (7) and (8) in Online Methods, mean for N = 7). **d,** Proportion of II to the sum of individual muscle MIs for spike rate

and timing terms of equation (7) (mean $\pm$ S.E.M., all muscle pairs excluding DLMs, n = 56). **e,f,** The proportion of II_{rate} or II_{timing} to the sum of the individual spike rate or timing MIs, respectively (mean for N = 7 individuals). **g,** Estimates of lower and upper bounds of motor program MI (gray box), proportional estimate of motor program MI (red line), and sum of individual muscle MIs (star) for each moth and the population average. **h,** Mean $\pm$ S.E.M. of the spike rate entropy (Equation (9)) and the total MI (N = 7).

Coordination is achieved through timing, not rate

Because timing is ubiquitous across all the muscles and encoding strategies are consistent, we next ask whether the coordination of multiple muscles utilizes primarily rate or temporal encoding, or a mixture of both. To do this, we first estimated the joint MI between the spiking activity of two muscles and the yaw torque (see Online Methods):

$$I(S_A, S_B; \tau) = I([S_{A,r}\ S_{B,r}]; \tau) + \sum_{i_A=1}^{S_{A,r_{max}}} \sum_{i_B=1}^{S_{B,r_{max}}} p(i_A, i_B) I([S_{A,t}\ S_{B,t}]; \tau | (i_A, i_B)) \quad (2)$$

Here, S_A and S_B are the spiking patterns from two different muscles. $S_{A,r}$ and $S_{B,r}$ represent spike rate for each of the two muscles. $S_{A,t}$ and $S_{B,t}$ represent the spike timing patterns for each muscle. i_A and i_B are the spike rate conditions for each muscle. Finally, $p(i_A, i_B)$ is the joint probability of the spike rate conditions.

Then, we estimated the interaction information (II) between two muscles [36]:

$$II = I(S_A, S_B; \tau) - (I(S_A; \tau) + I(S_B; \tau)) \quad (3)$$

Here, all variables are the same as defined above. If II is positive, then it indicates net synergistic information, or that the two muscles together reduce the entropy of the motor output more than the sum of their individual contributions. If II is negative, that indicates that information is net redundant between the two muscles. Redundancy or negative II indicates that there is coordination in the information content between the two muscles.

All pairwise combinations of muscles in the motor program have non-zero, negative II values (Equation (3)), indicating that there are net redundant interactions (Fig. 4a). We separated the contributions of rate and timing information to II as II_{rate} and II_{timing} (Equations (7) and (8) in Online Methods), and found that nearly all the shared information between muscles is encoded in spike timing (Fig. 4b,c; Supp. Fig. S5). The mean $\pm$ S.E.M. of the spike rate II is -0.023 $\pm$ 0.003 bits/ws, while the mean spike timing II is -0.56 $\pm$ 0.02 bits/ws. Muscles in the motor program are coordinated (negative II) through spike timing and not through spike rate.

It is possible that spike timing is more important for coordination than rate simply because spike timing encodes more information overall. To test this we scaled the spike rate and spike timing interaction information according to the total magnitude of spike rate and spike timing mutual information. Overall, 31.8 $\pm$ 0.9% of spike timing MI and 3.4 $\pm$ 0.9% of spike rate MI in individual muscles is shared in pairwise interactions (Fig. 4d). Even considering the smaller magnitude of spike rate MI in individual muscles, spike rate encodes almost no coordinated information (Fig. 4e,f). Based on how these muscles interact in pairwise combinations, it appears that rate encoding of each muscle is independent of other muscles in the motor program.

The motor program utilizes less than 10 bits/wing stroke

The significant coordination between muscles and the limited amounts of information in each individual muscle suggests that the motor program operates with no more than 10 bits of information per wing stroke. To assess this, we bounded the mutual information conveyed by the entire motor

program, taking into account the redundant information in the pairwise combinations of the muscles (Fig. 4g). Doing MI calculations for greater than 2 muscles is not tractable using the k-nearest neighbors method because of increasing data requirements (Supp. Fig. S6,S7). The II for each combination of muscles can be subtracted from the motor program to determine upper and lower bounds on motor program MI, as well as intermediate estimate an overall motor program MI by subtracting the expected proportion of redundant information (see Online Methods).

The comprehensive flight motor program uses a mutual information rate of 1.85 bits/ws to 9.47 bits/ws, with a best estimate of 7.89 bits/ws (Fig. 4g, mean of N = 7). Since the average truncated wing stroke length used in these calculations was 0.04 s, this equates to an information rate between 46.2 bits/s to 237 bits/s. Lacking other comprehensive motor program recordings it is difficult to compare the total moth flight program to other systems. Still the motor program of *Manduca* flight is limited to ten motor output channels each processing only a few bits of information per wing stroke. Complex motor behavior, like flight control, is accomplished with little information compared to estimates of information rates in sensory systems. While individual sensory neurons have comparable information rate to the hawk moth motor units (6-13 bits/s in RGCs [37] and 1-10 bits/s in olfactory receptors [38]), these systems have orders of magnitude more receptors, so the maximum information rate across the system is orders of magnitude higher (875,000 bits/s in the guinea pig retina [37]).

However in a functional sense this motor output still allows the moth to specify a large number of possible motor states. To estimate this we determined how many states in the empirical torque probability density function can be encoded by the total motor program using the direct method (see

Online Methods). The range of mutual information rates means the moth can specify its torque to one of 4 to 1076 states during each wing stroke. Clearly, the lower and upper limits are not realistic. The lower bound MI specifies too few states, while the upper bound MI assumes that all interaction information across the motor program is the same in all pairwise combinations of muscles. Given the intermediate estimate between the upper and lower bounds, the motor program MI can specify 483 ± 109 states of yaw torque (N = 7 individuals) on each wingstroke.

We also estimated the entropy in spike rate using the direct method (Equation (9)). Excluding the DLM, the maximum rate entropy in each muscle was as least as large as the total MI actually encoded (Fig. 4h). This means that under perfect transmission the motor program could be encoded strictly in rate.

Discussion

Shared timing and rate strategies for flight

By investigating a comprehensive, spike-resolved motor program, we show that temporal encoding is not a feature only of specialized motor units, but is an essential control strategy ubiquitously and consistently utilized for activation and coordination of muscles. There are few, if any, differences in encoding strategies between the various indirect and direct flight muscles controlling the wings (Fig. 2b, Fig. 3), despite their different modes of actuation and functional diversity [20]. However, information is not strictly in timing. All muscles encode information about yaw torque utilizing both precise spike

timing and spike rate (Fig. 3c-e), with the exception of the DLMs which only spike once per wing stroke during flight.

The overall strategy of the moth motor program involves individual muscles acting as mixed temporal and rate encoders. Rate codes can produce graded changes in muscle force and timing codes can change when and how much force is produced during the wing stroke depending on non-linear muscle properties, but the translation of the mixed encoding strategy into movement is not this simple[3]. A simple interpretation of spike rate as proportional to force magnitude is inconsistent with independent rate codes amongst the muscles in the coordinated motor program (Fig. 4b,e). We expect that different muscles coordinate their changes in force, yet we do not see coordinated changes in spike rate across muscles. Moreover the timing of individual muscle action potentials by as little as $\pm$ 4 ms can modulate the power output of the main downstroke muscle from 0% to 200% of normal [15]. *In situ* preparations of a wing elevator muscle in a locust, *Schistocerca nitens*, showed that changing either the spike timing or the number of spikes altered power output [39]. Steering muscles, like the basalar muscle in the blowfly *Calliphora vicina* can act by dissipating energy rather doing positive work and the timing of activation can modulate power [40]. By shifting when in the strain cycle a muscle spikes, timing can modulate force as much as rate in animals from cockroaches [41] to turkeys [42]. The complex transformation of motor unit spike patterns into force gives plenty of potential for both precise timing and rate to convey rich information to control movement.

An unexpected feature of the comprehensive motor program is the similarity of encoding strategy across all the motor units (Fig. 3). In contrast to our results, calcium imaging of the direct muscles

controlling the wings in flies showed evidence for two categories of muscle encoding: phasic muscles that are transiently active or tonic muscles that are continuously active [21]. Flies may utilize a dichotomy of exclusively phasic (rate encoded) and tonic (temporally encoded) muscles organized into mixed functional groups. In contrast, *Manduca sexta* utilizes individual muscles with mixed encoding strategies but distinct functions. Flies have multiple similarly sized muscles acting on the same sclerite. Hawk moths usually have a larger, functionally dominant muscle (or muscles sharing innervation) in the group of muscles attached to the sclerite (see Supplementary Text). *Drosophila* fly at wing beat frequencies an order of magnitude higher than *Manduca sexta* and *Schistocerca nitens*. Larger size and longer wingbeat periods might allow for a single mixed timing and rate motor unit to have more power to drive the sclerites. Flies also achieve mixed encoding strategies for every functional group of muscles, but seem to do so by having at least one phasic and one tonic muscle acting on each sclerite [21]. While phasic and tonic calcium activation does not have the resolution of precise spiking activity, it does show a separation of timescales and the potential for separated mechanisms for coordination across muscles. For example, the firing rate of power muscles changes with wing amplitude and phase shifts in the tonic firing of a basalar muscle correlate with changes in wing kinematics [43].

Recording a comprehensive, spike-resolved motor program during behavior is especially feasible in larger insects because the motor system has a relatively constrained number of motor units. A large number of spike-resolved motor units has been previously recorded in locusts [44], although an explicit analysis of temporal and rate encoding has not been done in this system. Each of the motor units in the moth conveys much more information than is typical in a vertebrate: $\sim$1 bit per 40 ms cycle in moth

flight (Fig. 2b) vs. ∼0.1 bit per 400 ms period in songbird respiratory muscle [17]. Vertebrate muscles tend to have many more motor units than invertebrates. However, even the number of motor units in vertebrate muscle are typically orders of magnitude fewer than neurons in the brain. We expect that mixed timing and rate codes will be found in vertebrates and other organisms, and that understanding the use of shared strategies will improve our ability to interface with neural systems.

Timing codes require precise patterning of motor output

Timing codes are inherently limited by precision, both in the degree to which a spike can be reliably specified by the nervous system and the degree to which it can be reliably translated by the muscle and skeletal machinery into differential forces [3]. The precise spiking of the indirect flight muscles has causal and functional consequences for turning down to the sub-millisecond scale [15]. We now understand that this extends across the entire motor program (Fig. 3b) and that coordination is achieved primarily thorough spike timing patterns across muscles (Fig. 2b). Timing codes, even at the millisecond scale, can have functional consequences for movement because of the non-linear interplay between the biomechanical properties of the muscle, which vary depending on history and current state, and neural activating signals [3].

Given the relative few spikes per wing stroke, spike count per period is interpreted as a rate code, but there can be a distinction between rate and spike count in slow bursting motor units with many spikes per cycle. In the slow cycle frequencies of the crustacean stomastogastric pyloric rhythm and walking stick insects, muscle force does not strictly follow rate encoding and depends on the specific number of

spikes [45]. Nonetheless, even some slow muscles such as the radula closer in *Aplysia* do show force dependence on specific patterns of spikes [46]. Timing codes are sometimes argued to be precise rate codes, but that would argue for drastic rate changes in a short time period in single spike codes, like the one present in the hawk moth DLM, and codes that depend on specific spike patterns [17]. Timing codes can be distinguished from rate codes by a specific pattern of spikes activated at a precise time in relation to a behavior[3].

It is still unknown how precise temporal motor unit codes arise from higher brain areas, the central nervous system, and motor circuits in the spinal or ventral nerve cord. Precise motor timing could come directly from precise sensory encoding via direct connections between sensory receptors and efferent units. In flies, gap junctions exist between precise haltere mechanoreceptors [47] and steering muscles [48], producing very fast reflexes, which in conjunction with fast feedback from wing mechanoreceptors, precisely patterns the activity of the first basalar muscle in *C. vizina* [49]. However these reflexes are still influenced by visual commands that have to incorporate feedback passing through a number of central nervous system synapses [50]. In locusts, mechanical feedback from the tegula, a sensory organ depressed during each wing stroke, produces phase resetting in the flight motor pattern which helps coordinate the fore and hind wings [51]. In moths, there are rapid mechanosensory pathways from the antenna [52], wings[53] and potentially other organs that can provide reafference of movement that could be used in timing. However the apparent millisecond scale resolution of the motor code poses a challenge even for neural processing that requires only a few synapses.

359 It is possible that precision exists even in central brain regions. Some pairs of bilateral muscles in
360 *Drosophila* are innervated by motor neurons that receive input from the same circuitry in the nerve cord
361 [54] which could give a proximal source of the left-right precision seen in *Manduca* downstroke muscles
362 [15], but this alone is unlikely to be sufficient to account for the extent of timing codes. Central brain
363 regions have typically been thought to encode information primarily by rate, but a cortical area for
364 vocalization in song birds does show millisecond scale precision in encoding [13]. Precision in the
365 peripheral motor system may also come from transforming a population code or remapping of
366 dynamics distributed over large populations of neurons [24]. Both the central nervous system and rapid
367 sensorimotor pathways in the periphery provide potential mechanisms for spike timing precision.

368 The importance of timing in motor control

369 The prevalence of temporal coding in the moth motor program is not merely due to a limitation in how
370 much information can be encoded in spike rate, since the spike rate entropy reported was high enough
371 to account for the total mutual information encoded by each individual muscle that spiked more than
372 once per wing stroke (Fig. 4h). For the DVM and SA muscles, spike rate would have to have no
373 transmission error due to its entropy being similar in magnitude to the total MI, but for the 3AX and BA
374 muscles, there could be transmission error and the spike rate would still account for the total MI. The
375 only muscle in the hawk moth flight motor program where the bandwidth of rate encoding is
376 necessarily limiting was in the DLM, which cannot encode spike rate information since it activates only
377 once per wing stroke.

While temporal codes are present both in faster, high frequency systems and slower, low frequency systems [3], rate is still utilized. The contribution of variable spike rate may be that it enables higher bandwidth for conveying temporal information due to having more spikes where the timing can vary, provided the motor program again has sufficient precision. Neural prosthetic devices and brain-machine-interfaces have led to improved algorithms for decoding motor implications of neural activity on a single-trial-basis [24, 55]. Such methods frequently assume that neural activity translates to motor behavior via a rate code. Since spike timing contains much more information than spike rate in every single muscle examined in a comprehensive motor program, incorporating spike timing or pattern information shows promise for improving decoding algorithms.

Analysis of rate alone may miss important structure in how brains pattern movement. For example, coordination of movement is achieved through the timing of muscle activation across a motor program, providing evidence which supports the existence of coordination specific to spike timing. Previous investigations of muscle synergies could not assess coordination at the spike level, though timing of muscle activation was an important component of the synergies identified in frogs, cats, and humans [25, 56, 57]. However, a majority of the information used to coordinate muscles may be overlooked by not considering spike timing. Not all information encoded by individual muscles was shared, supporting some measure of independent timing encoding and nearly entirely independent rate encoding (Fig. 4b). Accounting for shared information between muscles reduces the information in the comprehensive motor program, but still enables the encoding of 100s of unique states.

Sequences of muscle timings can also coordinate to reconfigure the motor system from one behavior to the another. This occurs during the transition from chewing to swallowing in *Aplyia*. The sea slug uses the same motor units to accomplish both behaviors but can switch between them with a shift in timing of muscle activation that is highly sensitive because the mechanical system is poised at a critical point in its dynamics [58]. In the moth motor program each muscle has a small amount of independent motor information it can convey with rate, while control encoded in timing is coordinated across multiple muscles. Reconfiguration of the motor system for different tasks may not require different levels of activation or change in rate, but rather changes in overall coordination of patterns in precise spike timings.

Millisecond level changes in the timing of neural firing have been shown in many different species to alter behavioral output [13–15]. Millisecond control acts on longer time scales over the course of cockroach strides [41], decision commands in fly escape flight [16], and in bird respiratory motor units [17]. Timing encoding in the most peripheral motor output may be the rule rather than exception and at least in moths also underlies how muscles form coordinated groups. Temporal encoding is not only relevant for single muscles, but is an essential control strategy consistently utilized for coordination and activation of muscles in a complete motor program.

References

1. Theunissen, F. & Miller, J. P. Temporal encoding in nervous systems: A rigorous definition. *Journal of Computational Neuroscience* **2,** 149–162 (1995).

2. Gerstner, W., Kreiter, a. K., Markram, H. & Herz, a. V. Neural codes: firing rates and beyond. *Proceedings of the National Academy of Sciences of the United States of America* **94,** 12740–12741 (1997).

3. Sober, S. J., Sponberg, S., Nemenman, I. & Ting, L. H. Millisecond spike timing codes for motor control. *Trends in Neurosciences* **41,** 644–648 (2018).

4. Birmingham, J. T., Szuts, Z. B., Abbott, L. F. & Marder, E. Encoding of muscle movement on two time scales by a sensory neuron that switches between spiking and bursting modes. *Journal of Neurophysiology* **82,** 2786–2797 (1999).

5. deCharms, R. C. & Merzenich, M. M. Primary cortical representation of sounds by the coordination of action-potential timing. *Nature* **381,** 610–613 (1996).

6. Reinagel, P. & Reid, R. C. Temporal coding of visual information in the thalamus. *Journal of Neuroscience* **20,** 5392–5400 (2000).

7. Mackevicius, E. L., Best, M. D., Saal, H. P. & Bensmaia, S. J. Millisecond precision spike timing shapes tactile perception. *Journal of Neuroscience* **32,** 15309–15317 (2012).

8. Lawhern, V., Nikonov, A., Wu, W. & Contreras, R. Spike rate and spike timing contributions to coding taste quality information in rat periphery. *Frontiers in Integrative Neuroscience* **5,** 1–14 (2011).

9. Egea-Weiss, A., Renner, A., Kleineidam, C. J. & Szyszka, P. High precision of spike timing across olfactory receptor neurons allows rapid odor coding in Drosophila. *iScience* **4,** 76–83 (2018).

10. Bülbring, E. Correlation between membrane potential, spike discharge, and tension in smooth muscle. *Journal of Physiology* **128,** 200–221 (1955).

11. Milner-Brown, H. S., Stein, R. B. & Yemm, R. Changes in firing rate of human motor units during linearly changing voluntary contractions. *The Journal of Physiology* **230,** 371–390 (1973).

12. Ferster, D. & Spruston, N. Cracking the neuronal code. *Science* **270,** 756–757 (1995).

13. Tang, C., Chehayeb, D., Srivastava, K., Nemenman, I. & Sober, S. J. Millisecond-scale motor encoding in a cortical vocal area. *PLoS Biology* **12,** e1002018 (2014).

14. Suvrathan, A., Payne, H. L. & Raymond, J. L. Timing rules for synaptic plasticity matched to behavioral function. *Neuron* **92,** 959–967 (2016).

15. Sponberg, S. & Daniel, T. L. Abdicating power for control: a precision timing strategy to modulate function of flight power muscles. *Proceedings of the Royal Society B: Biological Sciences* **279,** 3958–3966 (2012).

16. Von Reyn, C. R. *et al.* A spike-timing mechanism for action selection. *Nature Neuroscience* **17,** 962–970 (2014).

17. Srivastava, K. H. *et al.* Motor control by precisely timed spike patterns. *Proceedings of the National Academy of Sciences of the United States of America* **114,** 1171–1176 (2017).

18. Dickinson, M. H. & Tu, M. S. The Function of Dipteran Flight Muscle. *Comparative Biochemistry and Physiology Part A: Physiology* **116,** 223–238 (1997).

19. Burrows, M. *The Neurobiology of an Insect Brain Ch. 11* (Oxford University Press, Oxford, 1996).

20. Kammer, A. E. *Flying in Comprehensive Insect Physiology, Biochemistry and Pharmacology* (Oxford: Pergamon Press, Oxford, 1985).

21. Lindsay, T., Sustar, A. & Dickinson, M. The function and organization of the motor system controlling flight maneuvers in flies. *Current Biology* **27,** 345–358 (2017).

22. Jamali, M., Chacron, M. J. & Cullen, K. E. Self-motion evokes precise spike timing in the primate vestibular system. *Nature Communications* **7,** 1–14 (2016).

23. Ting, L. H. Dimensional reduction in sensorimotor systems: a framework for understanding muscle coordination of posture. *Progress in Brain Research* **165,** 299–321 (2007).

24. Churchland, M. M. *et al.* Neural Population Dynamics During Reaching. *Nature* **487,** 1–20. ISSN: 1878-5832 (2012).

25. d'Avella, A., Saltiel, P. & Bizzi, E. Combinations of muscle synergies in the construction of a natural motor behavior. *Nature Neuroscience* **6,** 300–308 (2003).

26. Ivanenko, Y. P., Poppele, R. E. & Lacquaniti, F. Five basic muscle activation patterns account for muscle activity during human locomotion. *Journal of Physiology* **556,** 267–282 (2004).

27. Usherwood, P. The nature of 'slow' and 'fast' contractions in the coxal muscles of the cockroach. **8,** 31–52 (1962).

28. Rheuben, M. B. Quantitative comparison of the structural features of slow and fast neuromuscular junctions in Manduca. *Journal of Neuroscience* **5,** 1704–1716 (1985).

29. Kammer, A. E. The motor output during turning flight in a hawkmoth, Manduca sexta. *Journal of Insect Physiology* **17,** 1073–1086 (1971).

30. Kammer, A. E. & Nachtigall, W. Changing phase relationships among motor units during flight in a saturniid moth. *Journal of Comparative Physiology* **83,** 17–24 (1973).

31. Rheuben, M. & Kammer, A. Structure and innervation of the third axillary muscle of Manduca relative to its role in turning flight. *Journal of Experimental Biology* **131,** 373–402 (1987).

32. Sponberg, S., Dyhr, J. P., Hall, R. W. & Daniel, T. L. Luminance-dependent visual processing enables moth flight in low light. *Science* **348,** 1245–1248 (2015).

33. Kraskov, A., Stögbauer, H. & Grassberger, P. Estimating mutual information. *Physical Review E - Statistical, Nonlinear, and Soft Matter Physics* **69,** 066138 (2004).

34. Holmes, C. M. & Nemenman, I. Estimation of mutual information for real-valued data with error bars and controlled bias. *arXiv.* doi:`arXiv:1903.09280[q-bio.QM]` (2019).

35. Eaton, J. L. *Lepidopteran Anatomy* (John Wiley & Sons Limited, Hoboken, NJ, 1988).

36. Timme, N., Alford, W., Flecker, B. & Beggs, J. M. Synergy, redundancy, and multivariate information measures: An experimentalist's perspective. *Journal of Computational Neuroscience* **36,** 119–140. ISSN: 15736873 (2014).

37. Koch, K. *et al.* How much the eye tells the brain. *Current Biology* **16,** 1428–1434 (2006).

38. Juusola, M. & Song, Z. How a fly photoreceptor samples light information in time. *Journal of Physiology* **595,** 5427–5437 (2017).

39. Mizisin, A. P. & Josephson, R. K. Mechanical power output of locust flight muscle. *Journal of Comparative Physiology A: Neuroethology, Sensory, Neural, and Behavioral Physiology* **160,** 413–419 (1987).

40. Tu, M. S. & Dickinson, M. H. Modulation of negative work output from a steering muscle of the blowfly Calliphora vicina. *Journal of Experimental Biology* **192,** 207–224 (1994).

41. Sponberg, S., Spence, A. J., Mullens, C. H. & Full, R. J. A single muscle's multifunctional control potential of body dynamics for postural control and running. *Philosophical Transactions Of The Royal Society Of London Series B-Biological Sciences* **366,** 1592–1605 (2011).

42. Roberts, T. J., Marsh, R. L., Weyland, P. G. & Taylor, C. R. Muscular force in running turkeys: the economy of minimizing work. *Science* **275,** 1113–1115 (1997).

43. Tu, M. & Dickinson, M. The control of wing kinematics by two steering muscles of the blowfly (Calliphora vicina). *Journal of Comparative Physiology A* **178,** 813–830 (1996).

44. Zarnack, W. & Möhl, B. Activity of the direct downstroke flight muscles of Locusta migratoria (L.) during steering behaviour in flight. *Journal of Comparative Physiology A: Neuroethology, Sensory, Neural, and Behavioral Physiology* **118,** 215–233 (1977).

45. Hooper, S. L., Guschlbauer, C., von Uckermann, G. & Büschges, A. Different motor neuron spike patterns produce contractions with very similar rises in graded slow muscles. *Journal of Neurophysiology* **97,** 1428–1444 (2006).

46. Zhurov, Y. & Brezina, V. Variability of motor neuron spike timing maintains and shapes contractions of the accessory radula closer muscle of Aplysia. *Journal of Neuroscience* **26,** 7056–7070 (2006).

47. Fox, J. L., Fairhall, A. L. & Daniel, T. L. Encoding properties of haltere neurons enable motion feature detection in a biological gyroscope. *Proceedings of the National Academy of Sciences of the United States of America* **107,** 3840–3845 (2010).

48. Fayyazuddin, A. & Dickinson, M. H. Haltere afferents provide direct, electrotonic Input to a steering motor neuron in the blowfly, Calliphora. *Journal of Neruoscience* **16,** 5225–5232 (1996).

49. Fayyazuddin, A. & Dickinson, M. H. Convergent mechanosensory input structures the firing phase of a steering motor neuron in the blowfly, Calliphora. *Journal of Neurophysiology* **82,** 1916–1926 (1999).

50. Chan, W. P., Prete, F. & Dickinson, M. H. Visual input to the efferent control system of a fly's "gyroscope". *Science* **280,** 289–292 (1998).

51. Wolf, H. The locust tegula: significance for flight rhythm generation, wing movement control and aerodynamic force production. *Journal of Experimental Biology* **182,** 229–253 (1993).

52. Sane, S. P., Dieudonné, A., Willis, M. A. & Daniel, T. L. Antennal mechanosensors mediate flight control in moths. *Science* **315,** 863–866 (2007).

53. Pratt, B., Deora, T., Mohren, T. & Daniel, T. L. Neural evidence supports a dual sensory-motor role for insect wings. *Proceedings of the Royal Society B: Biological Sciences* **284,** 20170969 (2017).

54. Sadaf, S., Reddy, O. V., Sane, S. P. & Hasan, G. Neural control of wing coordination in flies. *Current Biology* **25,** 80–86 (2015).

55. Pandarinath, C. *et al.* Inferring single-trial neural population dynamics using sequential auto-encoders. *Nature Methods,* 805–815 (2018).

56. Ting, L. H. & Macpherson, J. M. A limited set of muscle synergies for force control during a postural task. *Journal of Neurophysiology* **93,** 609–613 (2005).

532 57. Clark, D. J., Ting, L. H., Zajac, F. E., Neptune, R. R. & Kautz, S. A. Merging of healthy motor
533 modules predicts reduced locomotor performance and muscle coordination complexity post-stroke.
534 *Journal of Neurophysiology* **103,** 844–857 (2009).

535 58. Ye, H., Morton, D. W. & Chiel, H. J. Behavioral/systems/cognitive neuromechanics of
536 multifunctionality during rejection in Aplysia californica. *Journal of Neuroscience* **26,** 10743–10755
537 (2006).

End Notes

Acknowledgements The authors thank Mark Willis, Tom Daniel, Ilya Nemenman, and Sam Sober for helpful discussions. This material is based upon work supported by the National Science Foundation Graduate Research Fellowship under Grant No. DGE-1650044 and Grant No. DGE-1444932. This work was also supported by an NSF CAREER (PoLS – 1554790) to SS and a Klingenstein-Simons Fellowship in the Neurosciences to SS.

Author Contributions RC and SS developed experimental techniques. RC and JP conducted electrophysiological experiments. RC did spike sorting analysis. JP did data analysis. RC, JP, and SS wrote paper and made figures.

Competing Interests The authors declare no competing interests.

Online Methods

Animals. Moths (*Manduca sexta*) were obtained as pupae (University of Washington colony) and housed communally after eclosion with a 12-hour light-dark cycle. Naïve males and females (N = 7) were used in experiments conducted during the dark period of their cycle.

Electromyography (EMG) recordings from flight muscles. Moths were cold anesthetized before removing scales from the ventral and dorsal sides of their thoraxes. We made two small holes in the cuticle using insect pins and inserted two silver EMG wires to take differential recordings from the indirect power muscles and direct steering muscles on each side of the animal (Supp. Fig. S1). These 5 pairs of muscles together comprise a nearly complete motor program for hawk moth flight (see Supplementary Text). A common ground wire was placed in the abdomen.

Imaging of flight muscles. We imaged external placement of silver EMG wires to ensure we targeted the correct muscles (Supp. Fig. S2). We also conducted post-mortem dissections on a subset of animals to verify our placement of EMG wires. All images were captured with a Zeiss Stereo Discovery v.12 equipped with a Zeiss Axiocam 105 color camera.

Experimental set-up. We tethered moths with cyanoacrylate glue to a 3D-printed ABS plastic rod that was rigidly attached to a custom-made six-axis force-torque (F/T) transducer (ATI Nano17,

FT20157; calibrated ranges: F_x, F_y = ±1.00 N; F_z = ±1.80 N; τ_x, τ_y, τ_z = ±6250 mN-mm). After tethering the moths, they were given 30 minutes to adapt to dark light conditions and recover from the surgery at room temperature before starting experimental recordings. Signals from the EMG wires were amplified using a 16-channel AC amplifier (AM Systems Inc., Model 3500) before acquisition with a NI USB-6259 DAQ board. Gauge voltages from the F/T transducer were also acquired with a second NI USB-6259 DAQ board. Both the EMG and F/T transducer gauge voltages were sampled at 10000 Hz. Outputs from these DAQ boards were captured using MATLAB (MathWorks). F/T transducer voltages were transformed into force and torque values on axes centered at the point of attachment of the moth to the tether (the dorsal surface of the thorax).

Visual stimulus. An artificial robotic flower was used to provide visual stimulus to the moth during recording, as in previous studies of hawk moth flight control[1, 2]. The flower was actuated in a purely horizontal, 1 Hz sinusoidal trajectory using precisely controlled servo motors (Phidgets, Inc.) connected to a 12 V DC power supply. We only considered trials where the moth was tracking the robotic flower. Different patterns of muscle activity have been observed for different types of behaviors, so controlling for tracking flight was necessary to ensure that we were consistent in the motor strategy we were recording and analyzing[3, 4]. To determine whether the moth was tracking the flower, we recorded high speed video at 250 fps above the moth (FASTEC IL4; 50 mm lens). The working arena was illuminated with an 850-nm IR light (Larson Electronics). Black fabric and poster board were used to isolate the arena around the moth. We identified a tracking response based on the head motion, abdomen motion, and wing kinematics of the tethered moth in response to the flower's motion. For the

trials where a visual tracking response was present, we computed the power spectral density of the yaw torque that the moth produced to determine whether a peak at 1 Hz was present, which would indicate coherent motion with the flower. To ensure that this peak was not an artifact of the flower motion or other mechanical elements of our experimental set-up, we carefully isolated the F/T transducer from the robotic flower, speakers, and other vibrating machines in the experimental room.

Analysis of spike trains. We utilized Offline Sorter (OFS; Plexon) to detect the precise timing of spiking events in the EMG recordings from the 10 muscles. This program utilized a mixed detection method which first applied a threshold crossing method, and then identified the peak in a short time window after threshold crossing. OFS documented the timing of the threshold crossing of each spike. We manually supervised the threshold value, waveform length, and deadtime (inter-spike interval) to maintain accuracy of detection. We visually verified accurate and consistent spike detection. We combined trials from the same individual for mutual information (MI) analysis. For instances where multiple signals were present on a single channel, we compared the raw signals from multiple channels. We cross-referenced the literature considering typical shape and phase of each muscle signal (see Supplementary Text and Fig. S1) [3–7]. When necessary, we also high pass filtered data using a 4th order Butterworth filter with a 100 Hz cutoff.

Wing stroke alignment. The strain gauge voltages from the F/T transducer were transformed to calibrated forces and torques and translated to the point of attachment of the moth to the tether. Timings of muscle spikes during a wing stroke were referenced to the peak downward force in the z-direction

during each wing stroke cycle, which corresponded approximately to the zero-phase crossing of the yaw torque. The phase crossing was determined by filtering F_z with an 8th order Type II Chebychev filter with a pass band of 3-35 Hz, which captures the natural wing beat frequency of *M. sexta*, which in tethered preparations is approximately 20 Hz. Using this alignment, we segmented both the torque and EMG data into wing strokes. For all following analyses, the raw yaw torque signal was low-pass filtered with a 4th order Butterworth filter with a cutoff frequency of 1000 Hz.

Mutual information. While we sampled the yaw torque at 10000 Hz, we did not use all sample points in our MI estimates. To reduce the dimensionality of the yaw torque in each wing stroke, we did a principle components analysis (PCA) on the torque waveforms within each individual. The length of the waveforms was cut off at the length of the smallest duration wing stroke in each individual. An alternative sampling method was also tested where wing strokes were phase-normalized, and the yaw torque was sampled at several phases during the wing stroke. Both methods give similar results. We used the resulting scores of the first 2 principal components (PCs) in the MI estimation.

To determine the relative importance of rate and temporal encoding, we implemented a Kraskov k-nearest neighbors method of estimating MI previously used to analyze spikes from breathing muscles in songbirds [8–10]. This method estimates the spike rate MI before calculating additional spike timing MI using this formulation:

$$I(S;\tau) = I(S_r;\tau) + \sum_{i=1}^{S_{r,max}} p(S_r = i) I(S_t;\tau|S_r = i) \tag{4}$$

The neural signals present in both the rate and temporal codes of the spiking activity is S, and the yaw torque PCs are represented by the w x 2 matrix τ, where w is the number of wing strokes. The first term in the equation is the spike rate MI, which measures the MI between the yaw torque τ and the w x 1 matrix S_r, which represents the number of spikes in each wing stroke w. The last term in the equation is the spike timing MI, which is the weighted sum of MI estimates between the yaw torque τ and the spike timings S_t, a w x i matrix of the wing strokes where the spike count is equal to i. The maximum value of the spike count condition in all wing strokes is $S_{r,max}$. The estimates are weighted by the probability $p(S_r = i)$ for each spike count condition i.

The Kraskov k-nearest neighbors method of MI estimation relies on the selection of an appropriate number of nearest neighbors k [8–10]. To choose the value of k (the number of nearest neighbors) for our estimation, we estimated the MI across different values of k. In most cases our estimates were insensitive to choice of k (Supp. Fig. S3), but in some case too small of a k creates unstable estimates of MI. We chose k = 4 because it was the smallest value of k where estimates became stable in both k-space (Supp. Fig. S3). In data fractioning, 90% of muscles in all moths provided stable MI estimates in when the data sizes were halved (Supp. Fig. S4). A few particular incidences require the full data (example is S4), but the conclusion across muscles and moths were robust to data size. For all spike timing MI estimations, any spike count condition that occurred in less than k+1 wing strokes or fewer wing strokes than the dimensionality of S_t or τ were not included in the summation.

We estimated error in our spike rate MI estimates using the variance of $I(S_r, \tau)$ estimates in non-overlapping fractions (for N = 1-10, data split into equal 1/N sets) of each individual moth's data

set. To estimate error in spike timing MI estimates, using the same data fractioning described above, we found the variance of each calculation $I(S_t, \tau|i)$ and then propagated the error through the weighted mean of $p(S_r = i)$. Note that this method assumes no error in our estimation of the probability of each spike rate condition. All the error estimates we found are at least an order of magnitude lower than the MI values, and are lower than the S.E.M. across individuals for all cases except the estimation of $I(S_r, \tau)$ for the DLMs, which approach I = 0 (Supp. Table 1).

Pairwise MI and interaction information. To investigate how MI is encoded across muscles, we estimated the joint mutual information between different pairwise combinations of muscles and the yaw torque response:

$$I(S_A, S_B; \tau) = I([S_{A,r}\ S_{B,r}]; \tau) + \sum_{i_A=1}^{S_{A,r_{max}}} \sum_{i_B=1}^{S_{B,r_{max}}} p(i_A, i_B) I([S_{A,t}\ S_{B,t}]; \tau|(i_A, i_B)) \quad (5)$$

$I(S_A, S_B; \tau)$ is the pairwise MI, or the mutual information between the torque and the joint spiking activity of one muscle, S_A, and another muscle, S_B. The first term is the pairwise spike rate MI, the mutual information between the number of spikes in each wing stroke of each pair of muscles ($S_{A,r}$ and $S_{B,r}$) and the yaw torque PCs, τ. The second term is the pairwise spike timing MI, the weighted sum of pairwise MI estimates between the yaw torque τ and the spike timings of each muscle ($S_{A,t}$ and $S_{B,t}$) where the spike count in the first muscle is i_A and the spike count in the second muscle is i_B. $S_{A,r_{max}}$ and $S_{B,r_{max}}$ are the maximum value of the spike count condition for the first and second muscles, respectively. The estimates are weighted by the joint probability $p(i_A, i_B)$ of each possible pairwise spike count condition. As in the individual MI estimations, we used a value of k = 4 (Supp. Fig. S6). The

pairwise spike timing MI estimations did not include any joint spike count conditions that occurred in less than k+1 wing strokes or fewer wing strokes than the dimensionality of $[S_{A,t}S_{B,t}]$.

We estimated error in our pairwise spike rate MI estimates using the variance of $I([S_{r,A}\ S_{r,B}], \tau)$ and the same methods as our individual muscle MI estimates (Supp. Fig. S6, S7). To estimate error in pairwise spike timing MI estimates, using the same data fractioning described above, we found the variance of each calculation of the second term of the pairwise MI equation (Equation (5)) and then propagated the error through the weighted mean of $p(i_A, i_B)$. All the error estimates we found are again at least an order of magnitude lower than the pairwise MI values, and are lower than the S.E.M. across individuals (Supp. Table 2).

To compare the pairwise MI and individual muscle MIs, we used an interaction information measure [11]:

$$II = I(S_A, S_B; \tau) - (I(S_A, \tau) + I(S_B, \tau)) \tag{6}$$

II is the interaction information, which is the difference between the pairwise MI $I(S_A, S_B; \tau)$ (Equation (5)) and the sum of the individual muscle MIs (Equation (4)) for muscles A and B. If $II > 0$, then the pairwise MI is larger than the sum of the individual muscle MIs, and the interaction between these muscles is net synergistic in their prediction of yaw torque. There is more information present when the activity of both muscles are known together compared with when they are known separately. If $II < 0$, then the sum of the individual muscle MIs is larger than the pairwise MI, and the interaction between these muscles is net redundant in their prediction of the yaw torque. There is overlapping or shared information present when the activity of both muscles are known together.

We also calculated this measure for separated spike rate II and spike timing II. The spike rate interaction information is:

$$II_{rate} = I([S_{A,r}\ S_{B,r}], \tau) - (I(S_{A,r}, \tau) + I(S_{B,r}, \tau)) \tag{7}$$

This equation takes the spike rate terms from both the pairwise MI estimate (Equation (5)) and the individual muscle MI estimates (Equation (4)). In the same way, the spike timing interaction information is:

$$II_{timing} = \sum_{i_A=1}^{S_{A,r_{max}}} \sum_{i_B=1}^{S_{B,r_{max}}} p(i_A, i_B) I([S_{A,t}\ S_{B,t}], \tau | (i_A, i_B)) - \left(\sum_{i_A=1}^{S_{A,r_{max}}} p(i_A) I(S_{A,t}, \tau | i_A) + \sum_{i_B=1}^{S_{B,r_{max}}} p(i_B) I(S_{B,t}, \tau | i_B) \right) \tag{8}$$

Similarly to the full II, positive values of II_{rate} and II_{timing} indicate net synergistic interactions between muscles 1 and 2 and negative values indicate net redundant interactions between muscles 1 and 2.

Spike rate entropy and total motor program information. We estimated the entropy of spike rate using the direct method ([12, 13]):

$$H_r = -\sum_{i=1}^{S_{r,max}} p(S_r = i) log_2(p(S_r = i)) \tag{9}$$

This direct method estimates the entropy by the probability of each discrete state of the spike rate condition $S_r = i$ up to the maximum value of the spike rate, $S_{r,max}$. The entropy is maximized by a uniform distribution, and minimized if only one state or value of spike rate is present in the data.

To estimate the amount of information present in the motor program, we first calculated the sum of the total MI estimates of all muscles for each individual. This value does not account for redundancy, and

therefore is an overestimation of the actual amount of information present in the motor program. We used three methods to determine a range of possible values for the total motor program MI. The minimum, lower bound on the total motor program MI was calculated assuming all interaction information values represented independent shared information, so that the maximum possible amount of interaction information was subtracted from the sum of the individual muscle MIs. The maximum, upper bound on total program MI, MI_{max}, was calculated assuming all interaction information values represented dependent shared information, so only the highest redundancy value was subtracted from the sum of the individual muscle MIs:

$$MI_{max} = \sum_{A=1}^{10} I(S_A, \tau) - max(II(S_A, S_B; \tau) | A \neq B, B \in 1-10) \tag{10}$$

A and B represent each of the 10 muscles in the motor program. $I(S_A; \tau)$ is the total MI for each muscle A (Equation (4)) and $II(S_A, S_B; \tau)$ is the II for each possible combination of muscles (Equation (5)). To provide a single best estimate within this range, We assumed that the redundant information in the entire motor program was proportion the the fraction of MI in each muscle that was redundant. That is, we reduced the sum of total MIs by the ratio of II to MI across all muscle pairs:

$$MI_{MP} = (1 + < \frac{II(S_A, S_B; \tau)}{I(S_A; \tau) + I(S_B; \tau)} >) \sum_{A=1}^{10} I(S_A, \tau) \tag{11}$$

where MI_{MP} is the final estimate for the total motor program MI. The maximum possible yaw torque entropy for each moth data set was determined by the number of wing strokes w recorded for that individual:

$$H_{\tau,max} = log_2(w) \tag{12}$$

To estimate how precisely the motor program MI could define different states of yaw torque output, we used direct method estimations on the joint probability distribution of the yaw torque PCs for decreasing bin sizes. This was used to determine the entropy when the motor output was divided into that number of states. Once $H_{\tau,max}$ was reached, we did not estimate the entropy for smaller bin sizes. This gave a mapping between the number of yaw torque states and the yaw torque entropy. The motor program MI encodes information about yaw torque entropy, so this was used to estimate how many states of yaw torque can be differentiated or controlled by the spiking activity of the muscles under perfect transmission from spikes to yaw torque states.

Data availability The data used in this paper will be made available on Dryad (accession information upon publication).

References

1. Sponberg, S., Dyhr, J. P., Hall, R. W. & Daniel, T. L. Luminance-dependent visual processing enables moth flight in low light. *Science* **348,** 1245–1248 (2015).
2. Stöckl, A. L., Kihlström, K., Chandler, S. & Sponberg, S. Comparative system identification of flower tracking performance in three hawkmoth species reveals adaptations for dim light vision. *Philosophical Transactions of the Royal Society B* **372,** 20160078 (2017).
3. Kammer, A. Motor patterns during flight and warm-up in Lepidoptera. *Journal of Experimental Biology* **48,** 89–109 (1968).
4. Kammer, A. E. The motor output during turning flight in a hawkmoth, Manduca sexta. *Journal of Insect Physiology* **17,** 1073–1086 (1971).
5. Kammer, A. E. & Nachtigall, W. Changing phase relationships among motor units during flight in a saturniid moth. *Journal of Comparative Physiology* **83,** 17–24 (1973).
6. Kammer, A. E. *Flying in Comprehensive Insect Physiology, Biochemistry and Pharmacology* (Oxford: Pergamon Press, Oxford, 1985).

731 7. Rheuben, M. & Kammer, A. Structure and innervation of the third axillary muscle of Manduca
732 relative to its role in turning flight. *Journal of Experimental Biology* **131,** 373–402 (1987).

733 8. Kraskov, A., Stögbauer, H. & Grassberger, P. Estimating mutual information. *Physical Review E -*
734 *Statistical, Nonlinear, and Soft Matter Physics* **69,** 066138 (2004).

735 9. Srivastava, K. H. *et al.* Motor control by precisely timed spike patterns. *Proceedings of the National*
736 *Academy of Sciences of the United States of America* **114,** 1171–1176 (2017).

737 10. Holmes, C. M. & Nemenman, I. Estimation of mutual information for real-valued data with error
738 bars and controlled bias. *arXiv.* doi:arXiv:1903.09280[q-bio.QM] (2019).

739 11. Timme, N., Alford, W., Flecker, B. & Beggs, J. M. Synergy, redundancy, and multivariate
740 information measures: An experimentalist's perspective. *Journal of Computational Neuroscience* **36,**
741 119–140. ISSN: 15736873 (2014).

742 12. Steveninck, R. R. D. R. V. *et al.* Reproducibility and Variability in Neural Spike Trains. **275,**
743 1805–1808 (1997).

744 13. Strong, S. P., Koberle, R., de Ruyter van Steveninck, R. R. & Bialek, W. Entropy and information in
745 neural spike trains. *Physical Review Letters* **80,** 197–200 (Jan. 1998).